Article

Towards a physically consistent phase-field model for alloy solidification

Peter C. Bollada [1,†]*, Peter K. Jimack [2,†] and Andrew M. Mullis [1,†]

[1] School of Chemical and Process Engineering; University of Leeds
[2] School of Computing; University of Leeds
* Correspondence: p.c.bollada@leeds.ac.uk
† These authors contributed equally to this work.

Abstract: We summarise contributions made to the computational phase-field modelling of alloy solidification from the University of Leeds spoke of the LiME project. We begin with a general introduction to phase-field, and then reference the numerical issues that arise from solution of the model, before detailing each contribution to the modelling itself. These latter contributions range from controlling and developing interface-width independent modelling; controlling morphology in both single and multiphase settings; generalising from single to multi-phase models; and creating a thermodynamic consistent framework for modelling entropy flow and thereby postulate a temperature field consistent with the concepts of, and applicable in, multiphase and density-dependent settings.

Keywords: Phase-field; alloy solidification; non-equilibrium thermodynamics; intermetallics

1. An introduction to phase-field modelling

Solidification of metals and alloys can be modelled using non-equilibrium thermodynamics. The principle difference between non-equilibrium and equilibrium thermodynamics being the existence of fields, such as temperature or concentration, that change in time. Phase-field modelling adds another principle field, so designed to provide a parameter which changes rapidly, but continuously, between the phases of matter of interest.

For pure metal solidification the principle field is the temperature field, T, but for alloy solidification the principle field is the conserved solute concentration field, c, and T often plays a less important role - see, for examples, [1–3]. The phase-field symbol, ϕ, and its multiphase relations, $\phi_i, i \in [1, n]$ when $n > 2$, is an example of an order parameter which typically takes the value of one in each of the phases of matter. For example, for two phases, $\phi_1 = 1$ may represent the liquid phase and $\phi_2 = 1$ the solid phase. Since the material must be one or the other, we have the constraint, $\phi_1 + \phi_2 = 1$, and it becomes more convenient to use the single symbol, ϕ with its extreme values representing two phases, e.g. $\phi = 1$ liquid, and $\phi = 0$ the solid. But in general there can be more than one solid phase necessitating a multiphase formulation (in which case $\Sigma_{i=1}^{n} \phi_i = 1$). It is often stated that the role of ϕ is to track the surface of solid growth. Though this is one of its roles, its other major role is to express the free energy associated with the surface. For a more detailed review of the role of phase-field modelling in solidification the reader may consult [4].

A distinction brought into sharp focus in the work of [5] is that of the division of all classical physical phenomena into conserved and non-conserved (or dissipative) energy systems. The principle behind much of phase-field modelling is the principle of optimal free energy minimisation, which firmly establishes phase-field solidification as modelling dissipative phenomena. The word "optimal" is crucial, since without it the principle is ill defined. The main objective of phase-field modelling of solidification is

Preprints (www.preprints.org) | NOT PEER-REVIEWED | Posted: 21 December 2021 doi:10.20944/preprints202112.0346.v1

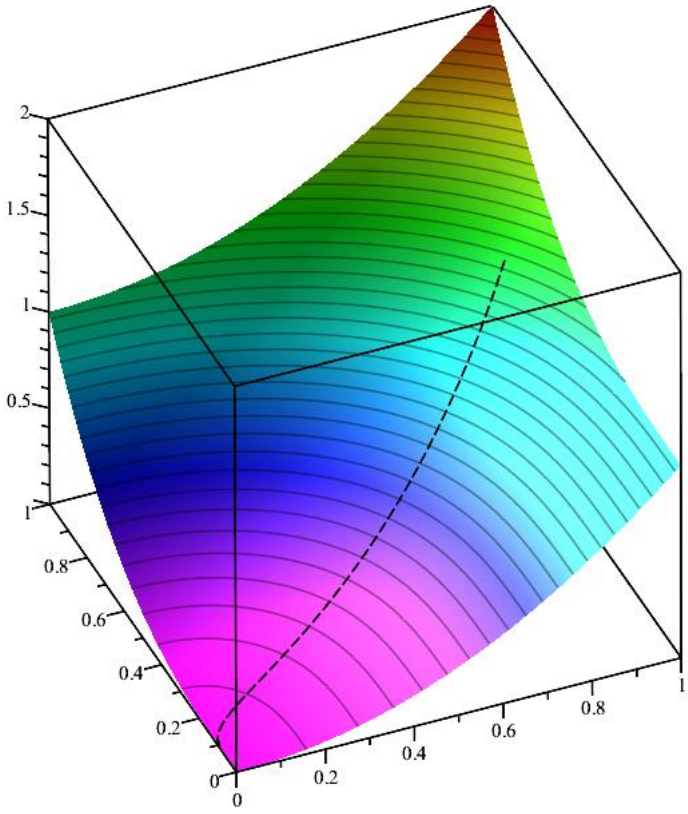

Figure 1. A path down a hill side following the path of steepest descent. The descending particle moves more quickly when the slope is steep (towards the top in this case) but slows down as it approaches a local minimum (near the bottom in this case).

to give insight into the role of free energy minimisation in the resulting morphology of solidifying melts. The modelling consists of three fundamental features: (1) Formation of the free energy in terms of the variables; (2) Specification of the diffusion parameters of the system; (3) Formation of the equations of motion by gradient descent of the free energy. A useful analogy for this process is that of descending down a hillside by, at each instant, choosing a path of steepest gradient and moving at a speed proportionate to the gradient. For the hill side analogy the two dimensional equations would be

$$\dot{\mathbf{x}} = -M\nabla h \tag{1}$$

or, in component form,

$$\dot{x_i} = -M\frac{\partial h}{\partial x_i}, i = 1,2 \tag{2}$$

Here x_1, x_2 are the two Cartesian directions in space, (more conventionally denoted x, y and (z for 3D), which we will use interchangeably with x_i where convenient); $\dot{\mathbf{x}}$ is the velocity; h is the height in coordinates x_1, x_2; and the parameter, $M > 0$, which may be a function of x_1 and x_2, controls the response to the driving gradient ∇h. Also notice the negative sign that enforces reduction rather than an increase in height. Such a descent is illustrated in Figure 1 following the dashed line which is always perpendicular to contours of equal height.

The phase equation for the evolution of ϕ is very similar in form:

$$\dot{\phi} = -M\frac{\delta F}{\delta \phi}, \tag{3}$$

where M controls the speed of descent - the mobility. F is the free energy of the domain as a whole. In 3D this is

$$F = \int f(\phi, c)\, \mathrm{d}x_1\, \mathrm{d}x_2\, \mathrm{d}x_3 \tag{4}$$

where the free energy density, f, is given in general by gradients and functions of ϕ and c (and also T if necessary). Variational techniques (using the notation discussed in [5]) convert the variational notation into functions of phase, ϕ, and its gradients, $\nabla\phi$:

$$\frac{\delta F}{\delta \phi} = -\nabla \cdot \frac{\partial f}{\partial \nabla \phi} + \frac{\partial f}{\partial \phi}. \tag{5}$$

In Eq. 1, the path has two degrees of freedom. On the other hand, since the function, $\phi(\mathbf{x}, t)$, is defined by all its values throughout the 2D (or 3D) domain, Eq. 3 has infinite degrees of freedom. To understand this consider ϕ to be approximated by its value at N points, Φ_i, for $i = 1..N$. Then this system would involve N degrees of freedom, with equations

$$\dot{\Phi}_i = -M\frac{\partial F}{\partial \Phi_i},\ i = 1..N \tag{6}$$

where the similarity with the component form of hill descent, Eq. 2, is clear.

In this way, the specification of F, being the integral of the density, f, across the whole domain leads towards a field equation which gives the evolution of ϕ at every point . By design, one feature of the phase is that it is not a conserved quantity in solidification. Non-conservation of phase is essential to allow the liquid phase to be replaced by the solid phase as solidification progresses. For the solute concentration, a similar equation to Eq. 5 would lead to the undesirable consequence of an increase in one of the components of the binary alloy. To that end a Cahn-Hilliard equation in the form

$$\dot{c} = \nabla \cdot D\frac{\partial f}{\partial c} \tag{7}$$

is used for solute evolution (typically, gradients of solute, c, are not used in the formation of free energy). Here D is the solute diffusion which is always (for substitutional diffusion) several orders smaller in the solid than in the liquid, and written (in the two phase case) $D = \phi D_{\mathrm{Liquid}} + (1-\phi)D_{\mathrm{Solid}}$, where $D_{\mathrm{Liquid}} \gg D_{\mathrm{Solid}}$.

2. Numerical techniques

Once the free energy density is specified, the evolution equations are known given initial conditions. For binary alloy models the phase-field initial condition consists of an initial nucleus, without which the system would remain in a permanent metastable state of undercooled liquid. This nucleus must be the solid phase (not just a surface such as a boundary or another phase). The initial condition for solute consists of a boundary value and often a value which differs in the solid region.

The evolution equations can rarely be solved analytically, even in 1D. Considerable computational resources are frequently required alongside state-of-the-art numerical techniques. Two factors make the solution problematic: one, the equations are non-linear; two, there is a lot of activity on the growing surface but the field throughout a large proportion of the domain is also required. If both solute and temperature equations are added to the phase equations, realistic diffusion parameters stretch the size of the

Preprints (www.preprints.org) | NOT PEER-REVIEWED | Posted: 21 December 2021 doi:10.20944/preprints202112.0346.v1

domain to orders of magnitude larger than the solid region. The surface itself is often fractal in appearance, so even if a locally adaptive grid is used the degrees of freedom can be prohibitive, see [6] for a detailed discussion of numerical techniques brought to bear on model of [3].

There are a number of numerical techniques in operation in the solution of such equations. One in particular is the treatment of non-linearity, see [7]. This typically, involves linearising the system locally, using the derivative of terms in the evolution equations. This can lead to complicated analytical expression which are model dependent. That is, these terms will often change when a new material is introduced, say, from AlCu to AlFe - or even changing from a physically realistic data based model to a more convenient simpler approximation. Because of this we choose to work with a numerical derivative for the linearisation, making the computer code much more flexible without compromising the solution techniques. Finally, because of the high number of degrees of freedom, the use of parallel computing becomes essential and the load balancing, across possibly thousands of nodes, becomes an issue, see [8]. Note that the contributions of [7,8], whilst using phase-field simulation as the motivation, are primarily around our development and understanding of numerical methods that can be applied to a much wider class of time-dependent problems - see [9].

3. Free energy formation

For simplicity of exposition we focus now on systems with only two phases present. Multiphase will be revisited briefly in Sec. 6 and subsequently Sec 9.

Formation of the free energy density, f, is where much of the modelling takes place. The free energy density is a sum of two parts: the surface, f_S, and the bulk, f_B:

$$f = f_S(\nabla\phi, \phi, c) + f_B(\phi, c) \tag{8}$$

For the simplest binary alloy model, f_S is given by

$$f_S = \frac{1}{2}\delta^2 \nabla\phi \cdot \nabla\phi + \frac{1}{2}\phi^2(1-\phi)^2 \tag{9}$$

where δ has the units of length and is associated with the thickness of the transition region between liquid and solid (here and throughout this article we use a dimensionless form for energy for simplicity of expression - see Appendix A). This model gives isotropic growth. The first term (containing the gradient) gives a penalty for a gradient in phase, which, if acting alone, would destroy the initial condition and melt the alloy. The other term known as the double well potential, $\Omega \equiv \frac{1}{2}\phi^2(1-\phi)^2$ (both non gradient and non-linear), has the opposite effect and, acting alone, would intensify the gradient towards infinity. The two terms acting together give a reasonably constant interface thickness with a transition well approximated by the shape illustrated in Figure 2 (see also Eq. 13).

4. Phase profile

Considering just the surface contribution in 1D so that

$$F_S = \int f_S \, \mathrm{d}x = \int \left[\frac{1}{2}\delta^2 \frac{\partial\phi}{\partial x}^2 + \frac{1}{2}\phi^2(1-\phi)^2 \right] \mathrm{d}x \tag{10}$$

then setting the variational derivative of this to zero,

$$\frac{\delta F_S}{\delta \phi} = 0, \tag{11}$$

Preprints (www.preprints.org) | NOT PEER-REVIEWED | Posted: 21 December 2021 doi:10.20944/preprints202112.0346.v1

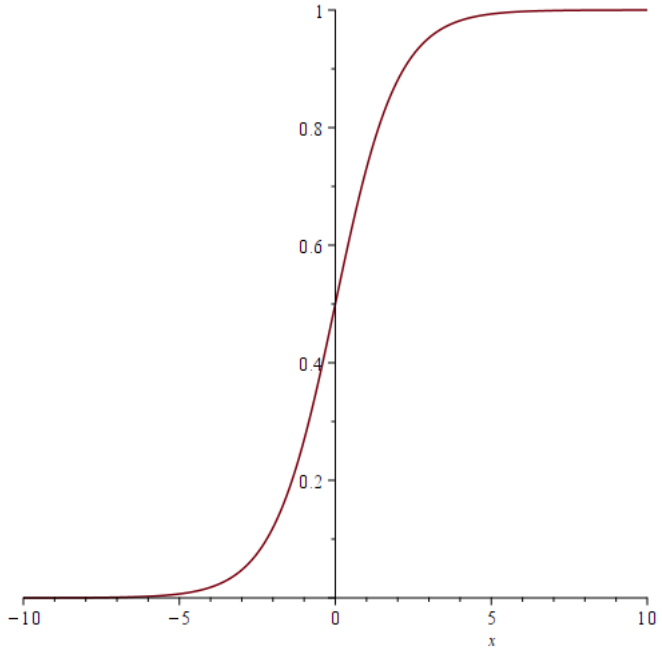

Figure 2. Phase profile showing the gradual transition from the solid phase on the left to the liquid phase on the right. Formally, the surface is at $x = 0$

implies the differential equation:

$$\delta^2 \frac{\partial^2 \phi}{\partial x^2} = \frac{\partial}{\partial \phi}\left[\frac{1}{2}\phi^2(1-\phi)^2\right] = 3\phi^2 - 4\phi + 1. \tag{12}$$

Eq. 12 is solved by the phase profile

$$\phi = \frac{1}{1+\exp(-x/\delta)}, \tag{13}$$

which is near zero for $x \ll 0$ and near unity for $x \gg 0$ with a transition region in proportion to δ about $x = 0$. The profile is illustrated in Figure 2 with $\delta = 1$, and means, in the absence of any driving force the shape of the phase-field satisfying just the surface contributions to the phase-field, is given by Eq. 13. This may prompt the question: How is the phase profile controlled in general, say to match a specific profile? Eq. 13 may be rearranged

$$\frac{x}{\delta} = \ln(1-\phi) - \ln\phi. \tag{14}$$

By considering a generalisation of Eq. 14 in the form of

$$X \equiv \frac{x}{\delta} = a_1 \ln(1-\phi) + a_2 \ln\phi + a_3 \tag{15}$$

it becomes possible to use the coefficients a_1, a_2 and a_3 to fit a desired profile to data from, say, a molecular dynamics simulation or *ab initio* calculation. As shown in [10], the form of the potential well, Ω, necessary for a skewed profile is given by

$$\Omega = \frac{1}{2}\left(\frac{\partial X}{\partial \phi}\right)^{-2} \tag{16}$$

Preprints (www.preprints.org) | NOT PEER-REVIEWED | Posted: 21 December 2021 doi:10.20944/preprints202112.0346.v1

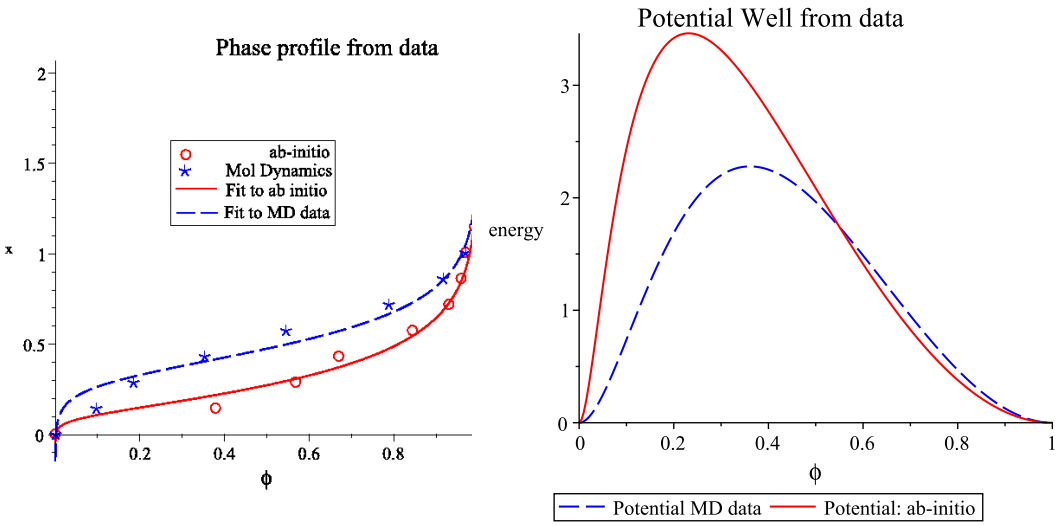

Figure 3. From data points on the left we fit two curves which result in the two potential wells in the right figure.

and the form for the interpolation polynomial, g, is given by

$$g(\phi) \propto \int \sqrt{\Omega}\, \mathrm{d}\phi \tag{17}$$

Derivation of these Equations is given in [10], where an application of the method to real data is shown in Figure 3.

5. Anisotropy

Anisotropy is typically introduced into phase-field models by the addition of an anisotropy term, $A(\nabla\phi)$ in the following manner

$$f_S = \frac{1}{2}\delta^2 A^2 \nabla\phi \cdot \nabla\phi + \frac{1}{2}\phi^2(1-\phi)^2 \tag{18}$$

The anisotropy, A, is dimensionless, but because of the presence of gradients in its definition, considerably adds to the non-linearity. Referring to an earlier point about model dependent terms in Sec. 2, changing the anisotropy changes the linearisation in the numerical scheme. In phase-field modelling literature, probably the most explored form of A is that of the 2D four-fold anisotropy (not withstanding its limited use in nature, since 2D systems are rare):

$$A = 1 + \epsilon\cos(4\theta) \tag{19}$$

where the new variable, θ, is related to the phase variable

$$\cos\theta = \frac{\phi_x}{\sqrt{\phi_x^2 + \phi_y^2}} \tag{20}$$

where ϕ_x, ϕ_y is shorthand for the x and y derivative of ϕ respectively. The effect of this example of A is to give a small preferential growth direction along the Cartesian x and y axes. When the driving force is strong this results in highly directional growth – dendrites (see Figure 4 illustrating 3D growth using an extension of the anisotropy model Eq. 19). Emergence of these highly complex morphologies continues to excite phase-field modellers to date. For example, it is possible with highly parallel computers to simulate a large number of dendrites with different preferential growth directions, [11].

Preprints (www.preprints.org) | NOT PEER-REVIEWED | Posted: 21 December 2021 doi:10.20944/preprints202112.0346.v1

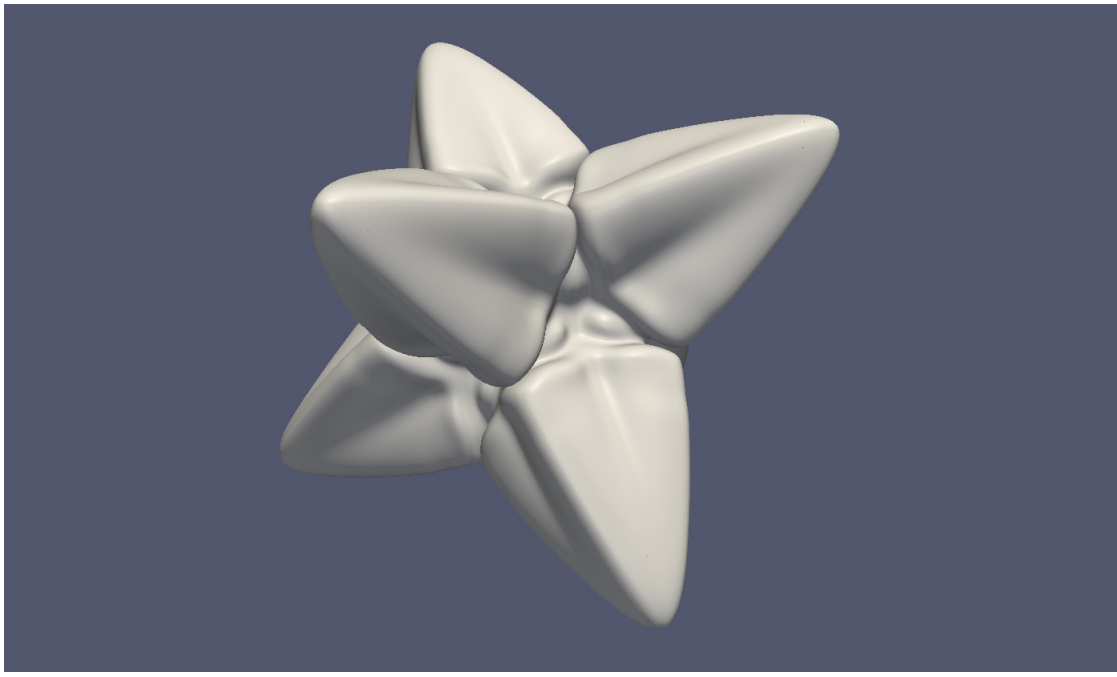

Figure 4. Dendrite growth with a 3D extension of the model anisotropy given in Eq. 19

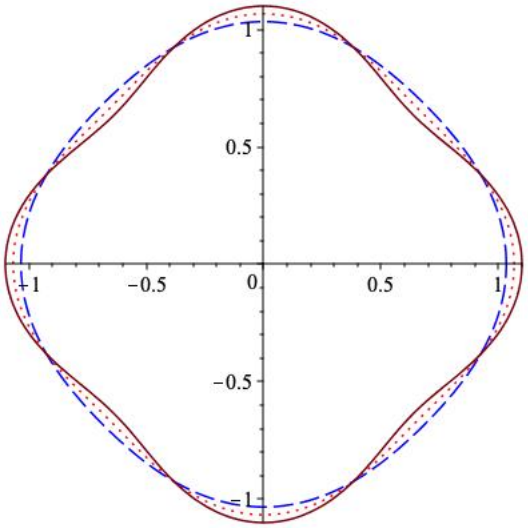

Figure 5. A polar plot of the anisotropy function Eq. 19 for a range of values: $\epsilon = 1/30, 1/15, 1/10$. Which are, respectively: dashed blue; dotted red; and solid brown. For values of $\epsilon < 1/15$ the polar plot has positive curvature but for values of $\epsilon > 1/15$ the plot develops points of inflection.

Preprints (www.preprints.org) | NOT PEER-REVIEWED | Posted: 21 December 2021 doi:10.20944/preprints202112.0346.v1

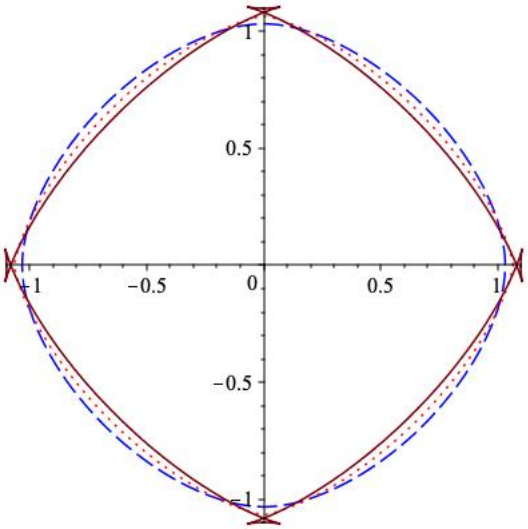

Figure 6. A Wulff plot of the anisotropy function Eq. 19 for a range of values: $\epsilon = 1/30, 1/15, 1/10$. Which are, respectively: dashed blue; dotted red; solid brown. For values of $\epsilon < 1/15$ the Wulff shape is continuous but for values of $\epsilon > 1/15$ the plot develops cusps (in the solid brown line)

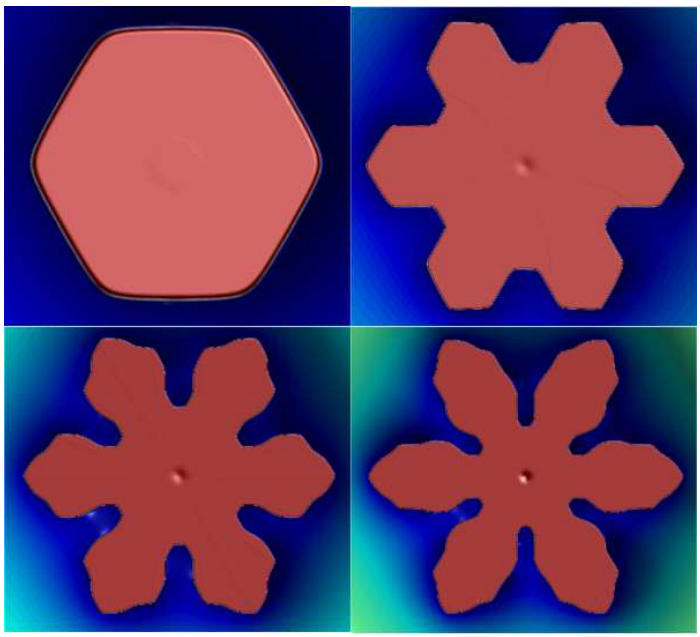

Figure 7. Clockwise from top left, the morphology for $T = 1300$K, $T = 1200$K, $T = 1000$K and (bottom left) $T = 1100$K. Each plot is a function of solute concentration, the solid being effectively pure metal ($c = 1$). The blue area around the crystal indicates concentration depletion close to the growing edge $c \sim 0.3$. for $T = 1000$K

Preprints (www.preprints.org) | NOT PEER-REVIEWED | Posted: 21 December 2021 doi:10.20944/preprints202112.0346.v1

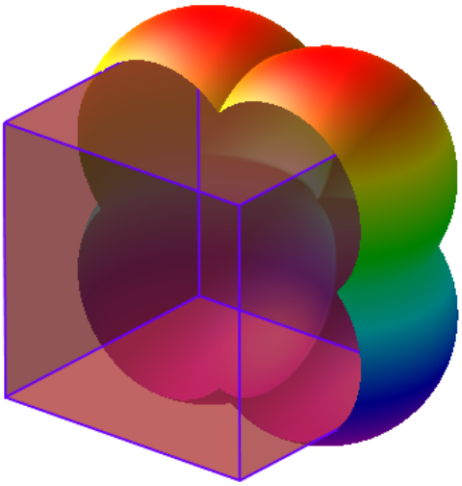

Figure 8. Anisotropy for a cube shown with half the anisotropy cut away. The cube vertices are at the points of maximum anisotropy and there is a cusp minimum at the centre of all faces

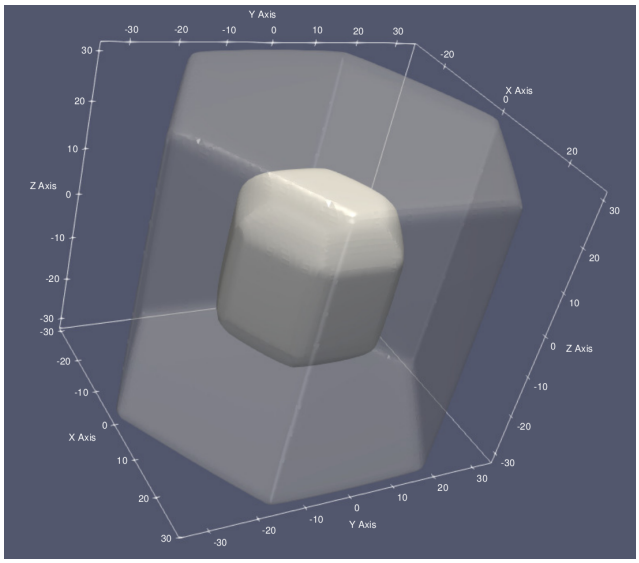

Figure 9. Mature hexagonal prism viewed in semi transparent perspective with an earlier growing crystal superimposed. The initial seed is a sphere of radius 10 and so the crystal growth forms the faceted faced before the edges and vertices.

Preprints (www.preprints.org) | NOT PEER-REVIEWED | Posted: 21 December 2021 doi:10.20944/preprints202112.0346.v1

The role of the parameter, ϵ, in the anisotropy is interesting. When $\epsilon = 0$ we return isotropy. However, there is a value, $\epsilon = 1/15$ in Eq. 19, beyond which the resulting predicted equilibrium morphology in unstable. At the critical value, the function develops points of inflection (see Figure 5). Now, it is widely known (and our paper, [12], discusses this) that a point of inflection in the anisotropy is associated with a discontinunuity in the associated equilibrium shape (also called the *Wulff* shape). The equilibrium shape, W, is given parametrically by

$$W(t) = [x = A(t)\cos t - A'(t)\sin t, y = A(t)\sin t + A'(t)\cos t] \tag{21}$$

and is illustrated with three values of ϵ in Figure 6

This has not prevented some researchers from using values of $\epsilon \gg 1/15$, with some stabilisation techniques in order to simulate faceted growth, [13–15]. After first following standard literature to explore the growth of a regular hexagon in [16] to investigate the transition from pure faceted to dendritic morphology (see Figure 7), we argue, in our paper [12] that there is a cleaner, more flexible approach to facet modelling. To introduce faceting into the model we first specify the vertices and give the following formula for anisotropy:

$$A = \max\left(\frac{\nabla\phi}{|\nabla\phi|}\cdot\mathbf{p}_i, i = 1..n\right) \tag{22}$$

where $\mathbf{p}_i$ are the n vertices of the resulting required equilibrium morphology. The quantity, $\mathbf{n} \equiv \nabla\phi/|\nabla\phi|$ is the normal to the surface, and so when the normal is in the same direction as one of the vertices, say, $\mathbf{p}_3$, then A takes on the magnitude of $\mathbf{p}_3$. For 2D shapes, A becomes a function of angle, θ and it is seen to be a series of connected circular arcs which pass through the vertices and meet on each facet. In 3D the surface energy is generalised to a series of connected spheres (see Figure 8). The real advantage of Eq. 22 is its flexibility to introduce any shape into phase-field, and then observe the growth towards the equilibrium shape (and beyond). For example, snapshots of the growth of a hexagonal prism are shown in Figure 9. Starting from a spherical seed we see the flat faces forming before the edges.

6. Bulk free energy

One of the more versatile forms of bulk free energy is that of an ideal binary solution, which consists of an entropy of mixing term plus a linear term for each phase (no Redlich-Kister terms):

$$f_i(c) = c\ln c + (1-c)\ln(1-c) + \Delta_i c + a_i \tag{23}$$

(see [17]) where Δ_i, a_i are given constants. A traditional method for combining these separate energies into a bulk free energy, f_B, is given by

$$f_B = \sum_{i=1}^{n} g_i f_i(c) \tag{24}$$

where, assuming a suitable interpolation function (i.e. monotonically increasing between $g(0) = 0$ and $g(1) = 1$, and with zero gradients at the extremes, $g'(0) = g'(1) = 0$),

$$g_i = \frac{g(\phi_i)}{\sum_{j=1}^{n} g(\phi_j)} \tag{25}$$

prescribes a set of normalized functions ($\sum_i g_i = 1$), for multiphase interpolation.

For two phase, the formulation of the bulk free energy reads

$$f = \frac{1}{2}A^2\delta^2\nabla\phi\cdot\nabla\phi + \frac{1}{2}\phi^2(1-\phi^2) + g(\phi)f_{\text{liq}}(c) + (1-g(\phi))f_{\text{sol}}(c) \tag{26}$$

Preprints (www.preprints.org) | NOT PEER-REVIEWED | Posted: 21 December 2021 doi:10.20944/preprints202112.0346.v1

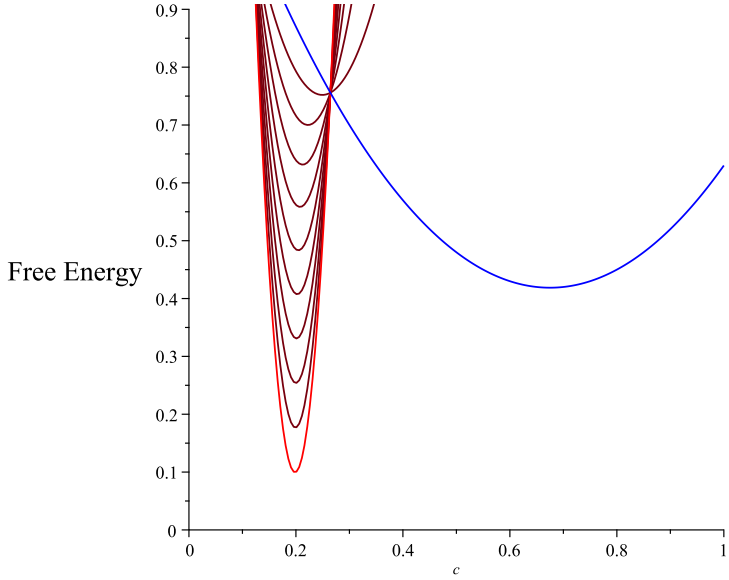

Figure 10. This figure illustrates the problem with using the methods of [17] when applied to intermediate values of ϕ between zero and one. The solid intermetallic (red) has a narrow range about 0.2 and the liquid a broader range. Interpolation between the two curves (the brown curves for equal values of $\phi = 0.1, 0.2, ..0.9$) is vertical and effectively creates an energy barrier where the two curves cross.

where $f_{\text{liq}}(c), f_{\text{sol}}(c)$ are the given bulk free energy densities for each phase of the binary alloy; possibly of the form given in Eq. 23.

7. Intermetallics

Intermetallics resist standard treatment within phase-field because of their restricted solubility. This shows itself thermodynamically in free energy functions of solute concentration, in which the free energy may be defined for a limited range of c. The most extreme example of this being the stoichiometric intermetallic (or line compound), in which the solid only exists at one composition (e.g. Al_3Ni). The most obvious way this presents problems for phase-field is at the surface where the phase is defined as a mixture of the solid, with limited range, c, and the liquid. One way of negotiating the problem is to approximate the intermetallic by a quadratic which agrees by Taylor expansion at a critical point, namely a common tangent point, c_S. But, in so doing, there can remain a large energy barrier between $f_{\text{solid}}(c_S)$ and $f_{\text{liquid}}(c_S)$, making the system energetically difficult to solidify when using Eq. 26 in combination with Eq. 24, and illustrated in Figure 10.

This problem was largely solved by [18] and later put on a sound theoretical basis by [20]. The method of [18] as illustrated in Figure 11 is most readily adopted when quadratic approximation is used, and is the method we adopt in [12] when simulating faceted growth. The most distinguishing feature of the method of [18], illustrated in Figure 11 is that all the intervening curves have a common tangent value, i.e. there is a line which is tangent to all curves. Noticing this latter feature of the [21] model, we suggested in [19], an alternative method for forming the intervening curves, which involves a straightforward linear translation of the curves illustrated in Figure 12. There are two advantages of the latter method, as compared with [18]: one, it readily applies to non-quadratic approximations; two, the intervening curves do not extend outside of the unit range, $c = 0$ to 1 if the two bulk curves do not extend outside this range. For method [19], the bulk free energy is given by:

$$f_B = g(1-\phi)\tilde{f}_S + g(\phi)\tilde{f}_L \tag{27}$$

Preprints (www.preprints.org) | NOT PEER-REVIEWED | Posted: 21 December 2021 doi:10.20944/preprints202112.0346.v1

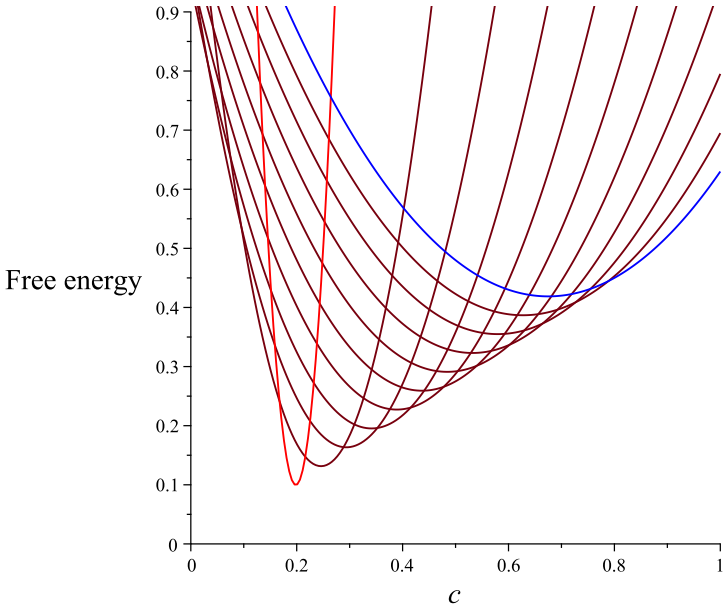

Figure 11. As in Figure 10 but with a different interpolation scheme. The transition between these two pure phases (in brown, as we move across the boundary between the two) is shown with the intervening curves. This is the method advocated by [18] for interpolating the two curves

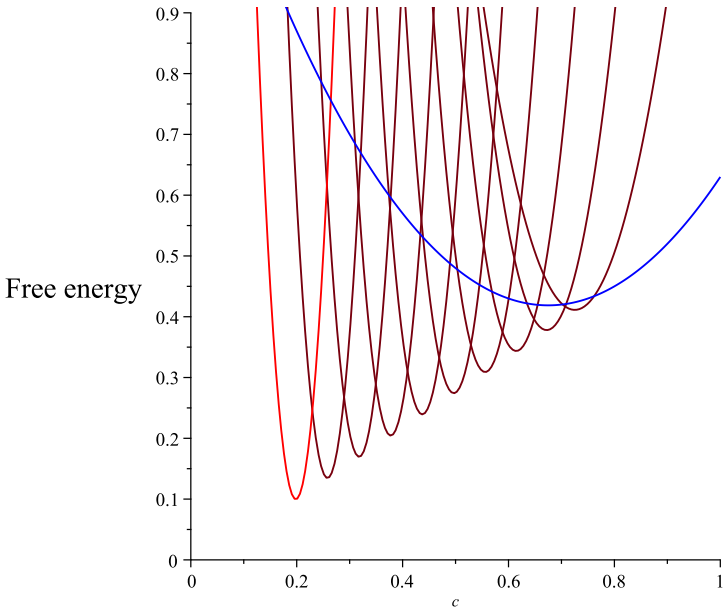

Figure 12. Here the free energy function of solute for an intermetallic in shown on the far left (red), together with the free energy curve of the liquid on the far right (blue). The transition between these two pure phases (in brown, as we move across the boundary between the two) is shown with the intervening curves. This is an alternative method suggested by [19] for interpolating the two curves

Preprints (www.preprints.org) | NOT PEER-REVIEWED | Posted: 21 December 2021 doi:10.20944/preprints202112.0346.v1

where

$$\begin{aligned}\tilde{f}_S &= f_S[c + g(\phi)(c_S - c_L)] - g(\phi)[f_S(c_S) - f_L(c_L)],\\ \tilde{f}_L &= f_L[c + g(1-\phi)(c_L - c_S)] - g(1-\phi)[f_L(c_L) - f_S(c_S)].\end{aligned} \tag{28}$$

That is, we use the equilibrium common tangent values c_L, c_S to specify the translations. Although this method does transition between solid and liquid smoothly between the original curves, it implies a very rapid change in the 2nd derivative near the liquid value, $\phi = 1$. This feature can be compensated for, but is (naturally) not present in the method of [18] illustrated in Figure 11 and, together with its theoretical underpinning [20], makes this the method of choice where possible.

8. Solute trapping

The previous section concludes that [18] is the method of choice for constructing the bulk free energy for intermetallic alloys. For less extreme free energy functions of fully soluble solids (i.e. not intermetallic), either the methods of [18] or [17] can be used successfully. That said, both methods still present an unresolved problem, for which this section puts forward a solution, applicable for both (and any) interpolation method. A key parameter in phase-field modelling is δ, the interface width. The value of δ may be given a physically real value, possibly arising from a molecular dynamic simulation. But often the value is dictated by choosing it small enough to capture features of the surface morphology. A physically real interface width usually implies that there is a very different characteristic length associated with the solute diffusion as compared with the interface width, resulting in many more grid points, less computational stability and significantly longer run times. Thus, a larger interface width, say, of the same order as the concentration length associated with diffusion (note, this also depends on growth speed) is computationally convenient but the influence of interface width on results must be then addressed. Writing the two-phase free energy, Eq. 26 in 1D we have

$$f = \frac{1}{2}A^2\delta^2\left(\frac{\partial\phi}{\partial x}\right)^2 + \Omega(\phi) + g(\phi)f_{\text{liq}}(c) + (1 - g(\phi))f_{\text{liq}}(c) \tag{29}$$

where Ω is the double well potential, e.g. $\Omega = \frac{1}{2}\phi^2(1-\phi)^2$, and derive equations of motion

$$\dot{\phi} = M\left[\delta^2\frac{\partial^2\phi}{\partial x^2} - g'(\phi)(f_{\text{liq}} - f_{\text{sol}})\right] \tag{30}$$

and

$$\dot{c} = \nabla \cdot D\nabla f_c = \partial_x(D\partial_x f_c) \tag{31}$$

where $f_c \equiv \frac{\partial f}{\partial c}$. We now assume that we have a phase profile of the form

$$\phi = \frac{1}{1 + \exp[-(x - Vt)/\delta]}, \tag{32}$$

that solves the 1D equation, Eq. 30 for some V and δ. Note that the slope of the phase-field is related to the interface width by

$$\left.\frac{\partial\phi}{\partial x}\right|_{x=0} = \frac{1}{4\delta}. \tag{33}$$

For the profile, Eq. 32, moving at constant speed, V, we have, $\frac{\partial}{\partial t} = -V\frac{\partial}{\partial x}$ so that

$$-V\partial_x c = \partial_x(D\partial_x f_c) \tag{34}$$

Preprints (www.preprints.org) | NOT PEER-REVIEWED | Posted: 21 December 2021 doi:10.20944/preprints202112.0346.v1

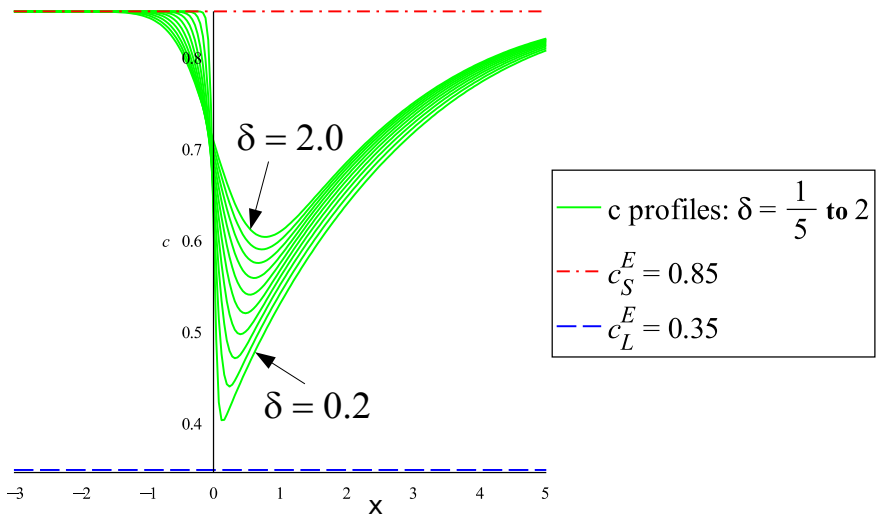

Figure 13. Example 1D steady state solutions to Eq. 35, for $V/D = 5$ for a given free energy, with various phase-field interface widths, $\delta = \frac{1}{5}, \frac{2}{5}, ..., 2$. None of the solutions here give the liquid equilibrium minimum, $c_L^E = 0.35$, ($\delta = 1/5$ is the closest, at ~ 0.4).

or

$$\partial_x(Vc + D\partial_x f_c) = 0 \tag{35}$$

Now, f_c is of generic form and phase dependent, so, given the boundary conditions for Eq. 35, it does not have ready solution. On applying numerical solution we find that we can fix the value of the solute in the solid and at infinity, but that the value in the interface arises from the solution - see Figure 13, which shows a value for c_L arising in the solution of the 1D problem for $\delta = 2$ of $c \approx 0.6$ and for $\delta = 0.2$ of $c \approx 0.4$. Both of which may be compared with the equilibrium value (or equivalently $\delta \to 0$) of $c = c_L^E$.

For two convex curves, there is a unique point on each curve such that

$$\frac{f_{\text{liq}}(c_L) - f_{\text{sol}}(c_S)}{c_L - c_S} = f'_{\text{liq}}(c_L) = f'_{\text{sol}}(c_S) \tag{36}$$

So, by choosing c_S as one boundary value, we find, as V decreases that the extreme value in the interface, c_L tends towards the common tangent value for the other function, f_{liq}. However, as shown in Figure 13, for $V > 0$ the result becomes dependent on $\delta \in [0.2, 2.0]$ with the maximum value of the solute profile falling short of the required value of c_L (assuming $c_L > c_S$). In [22] we show that it is possible to modify Eq. 35 to the form

$$\partial_x(Vc + D\partial_x f_c + D\alpha) = 0 \tag{37}$$

and demand that α is chosen such that $c_L = c_L^E$, for a given δ and V. By inspecting the dependency of α on both V and δ we find that the dependence is well approximated by

$$\alpha = \beta V \delta f_{c\phi} \phi'(x)/D_L \tag{38}$$

for some constant, β. In other words, finding β gives an anti-trapping current across a range of velocities, V, and interface widths, δ. We illustrate this in Figure 14 for a range $\delta = 0.1$ to 1, where β is chosen so that α is exact for $\delta = 1$.

Preprints (www.preprints.org) | NOT PEER-REVIEWED | Posted: 21 December 2021 doi:10.20944/preprints202112.0346.v1

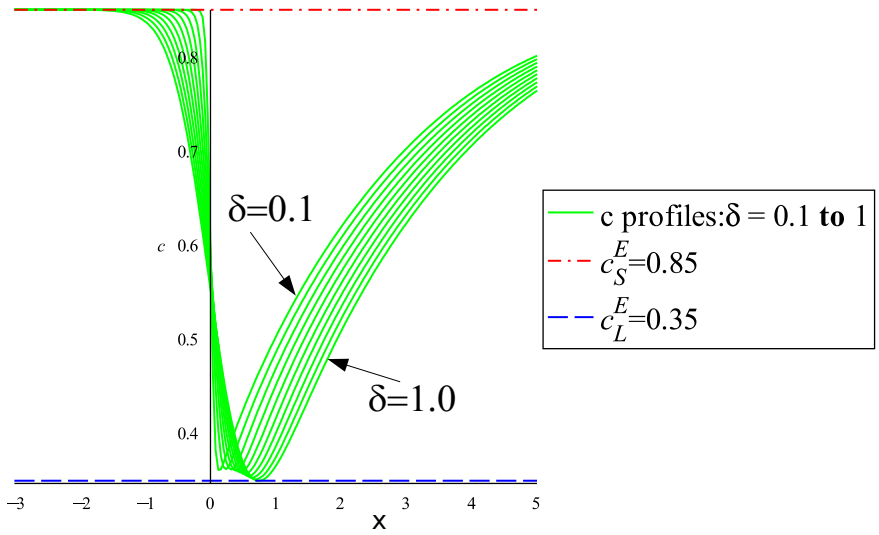

Figure 14. Solutions to the same steady state 1D problem as illustrated in Figure 13 but with an anti-trapping current. The value for $\delta = 1$ is chosen to be exact by the choice and for $\delta < 1$ the anti-trapping is approximate

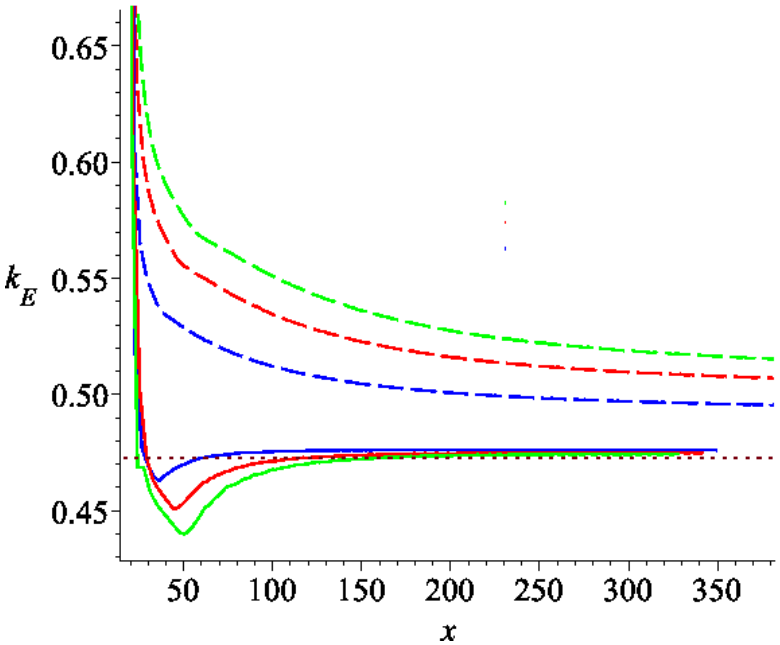

Figure 15. Here the lines represent the value $k_E \equiv c_{\text{sol}}/c_{\text{liq}}$ at a growing tip for three values of δ, for both the standard simulation (dashed), and the simulation with an anti-trapping current (solid), the interface-width, δ, is for as range with the largest (green) being twice the smallest (blue): $\delta/\sqrt{8} = 4, 6, 8$.

Preprints (www.preprints.org) | NOT PEER-REVIEWED | Posted: 21 December 2021 doi:10.20944/preprints202112.0346.v1

Using the value of V and δ at the tip of a growing dendrite in 2D or 3D, together with β, then allows us define a compensating current for use in two and three dimensions:

$$\mathbf{j} \equiv -\frac{D}{D_L} f_{c\phi} \beta \delta V \nabla \phi \tag{39}$$

to be used with a modified solute equation:

$$\dot{c} = \nabla \cdot (D \nabla f_c + \mathbf{j}) \tag{40}$$

Applying this model with physically realistic functions for liquid and solid phase PbSn we can extract the partition coefficient $c_{\mathrm{sol}}/c_{\mathrm{liq}}$ from the c field at the tip of a growing dendrite and compare with the equilibrium value and with changes in interface width δ. A plot of results is shown in Figure 15, where the dotted lines are without anti-trapping and the solid lines with the current in Eq. 40. The latter showing remarkable interface width independence and agreement with the equilibrium value. Without ant-trapping the solid lines are too high indicating that the value of c_{liq} is too high.

9. Eutectic modeling

A eutectic involves two solid phases growing symbiotically such that the growth of one solid phase reduces solute favourable to its growth, whilst leaving behind conditions favourable for growth of the other solid phase. Unlike single phase growth there is less of a build up of concentration at the growing surface. Initial models, e.g. [23] for multiphase were, in analogy with the single phase model, of the form

$$\dot{\phi}_i = -M \frac{\delta F}{\delta \phi_i}, \; i = 1..n \tag{41}$$

for n phases and given some suitable form for free energy density. But this form of the equations must be used in conjunction with a Lagrange multiplier (see also [23]) to avoid the constraint

$$\sum_i^n \phi_i = 1 \tag{42}$$

being violated. When a Lagrange multiplier is used it turns out that the form of the equations becomes

$$\dot{\phi}_i = -M_{ij} \frac{\delta F}{\delta \phi_j} \tag{43}$$

where the square matrix, $\mathbf{M}$ is given as a multiple of

$$\begin{bmatrix} 2 & -1 & -1 \\ -1 & 2 & -1 \\ -1 & -1 & 2 \end{bmatrix} \tag{44}$$

This guarantees that

$$\sum_i^n \dot{\phi}_i = 1 \tag{45}$$

and so with consistent initial conditions, Eq. 42 is satisfied for all time, t. Unfortunately, such a mobility matrix, Eq. 44, and its generalisation to $n > 3$ fails to reduce properly

Preprints (www.preprints.org) | NOT PEER-REVIEWED | Posted: 21 December 2021 doi:10.20944/preprints202112.0346.v1

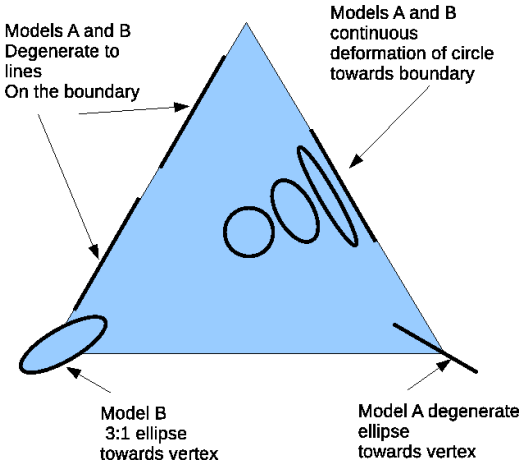

Figure 16. An illustration of the action of the mobility matrix given by Eq. 47. For comparison, the Lagrange multiplier approach would have every part of the region depicted as a circle (as in the centre of the triangle). On each edge, the two phase regions, the ellipses become degenerate

when only two of the $n > 2$ phases are present. A spurious phase will likely be generated. This is because, for example, with $\phi_1 = 0$:

$$\dot{\phi}_1 = -2\frac{\delta F}{\delta \phi_1} + \frac{\delta F}{\delta \phi_2} + \frac{\delta F}{\delta \phi_3} \tag{46}$$

the contribution from the second and third terms can be non zero. An alternative formulation, that we propose in [24], is to specify the mobility matrix as phase dependent

$$M_{ij} = -\frac{\phi_i \phi_j}{(1-\phi_i)(1-\phi_j)}, \; i \neq j \tag{47}$$

and

$$M_{ii} = -\sum_{j \neq i} M_{ij}. \tag{48}$$

To understand this form of matrix it helps to note that when only two phases are present the multiphase equations become identical to the single phase equations. Also, if there are equal amounts of each phase the matrix reduces to a multiple of Eq. 44 (used in Eq. 43). An illustration of the the mobility matrix is given in Figure 16 (model B - a more complicated, but similar, model - is also discussed in [24]).

For single phase the formation of the surface energy density for isotropic growth is given by Eq. 18. So, it is natural to postulate a multiphase surface energy density by the equation postulated in [23]:

$$f_S = \sum_{i=1}^{n} \frac{1}{2}\delta^2 \nabla\phi_i \cdot \nabla\phi_i + \frac{1}{2}\phi_i^2(1-\phi_i)^2 \tag{49}$$

where, indeed, this form reduces correctly when two phases only are present. As recognised at the time by the authors of [23], the form, Eq. 49 is not sufficiently general because the angles at the eutectic triple junction are enforced to be equal to 120°. This is insufficiently general, since the interfacial tensions between the three pairs of phases are usually unequal, and there is no provision (in Eq. 49) for the binary interaction of the surface energy between two phases. Another approach, which at least allows interfacial

Preprints (www.preprints.org) | NOT PEER-REVIEWED | Posted: 21 December 2021 doi:10.20944/preprints202112.0346.v1

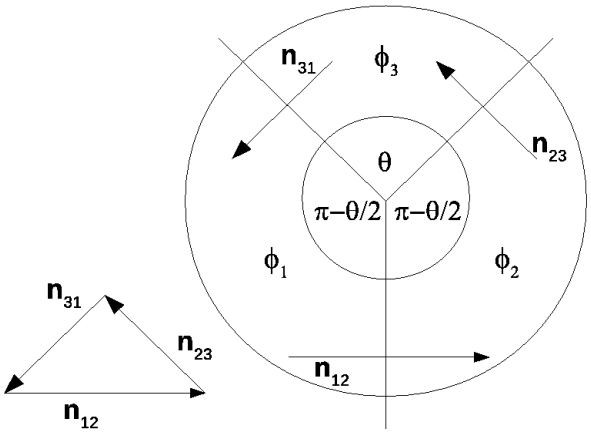

Figure 17. The relationship between junction angle and surface energy. These binary indexed proportions are then used to construct a single index which eneters the surface energy term in phase-field.

energies, $\sigma_{ij} \propto \delta_{ij}$, to be included, and also consistent with two phases, was proposed in [25] and [26] involving a double sum:

$$f_S = \sum_{i=1}^{n} \sum_{j \neq i}^{i-1} \frac{1}{2} \delta_{ij}^2 |\phi_i \nabla \phi_j - \phi_j \nabla \phi_i|^2 + \frac{1}{2} \phi_i^2 \phi_j^2. \tag{50}$$

It is not clear that the formulation Eq. 50 does actually control the angle at the junction. Some formulations introduce angle control by introducing an extra potential in the form of (for three phases), $\phi_1 \phi_2 \phi_2$ or its square, [27]. In [28] we propose a new formulation which gives direct control of the angle at the triple junction:

$$f_S = \sum_{i=1}^{n} \frac{1}{2} \delta_i^2 \nabla \phi_i \cdot \nabla \phi_i + \frac{1}{2} \phi_i^2 (1 - \phi_i)^2 \tag{51}$$

where as a consequence of a definition

$$\delta_{ij}^2 = \delta_i^2 + \delta_j^2. \tag{52}$$

the single indexed quantities may be written as a function of the double indexed quantities by

$$\delta_i^2 = \delta_{ij}^2 + \delta_{ik}^2 - \delta_{jk}^2, i \neq j \neq k. \tag{53}$$

Here, $\delta_{ij}, i \neq j$ is the surface energy between phase ϕ_i and ϕ_j. The relation of the surface energy to the angle at the triple junction is shown in Figure 17, which shows three lines containing three desired angles and then a triangle such that each side, n_{ij} crosses the lines at right angles. The relative lengths of the triangle sides is proportional to the quantities, δ_{ij} . To get a feel for the formulation set the two solid interface widths $\delta_2 = \delta_3 = 1$, then when δ_1 (the liquid) is equal to unity the formulation Eq. 49 is returned, but when $\delta_1 > 1$ the angle in the liquid area begins to increase past 120°, with the other two equal regions decreasing accordingly. Using a surface energy defined by Eq. 51 in phase-field gives the desired angle control as shown in Figure 18.

The construction of the multiphase model was greatly aided by the postulation of triple junction field, a function of three phases, which allows inspection of the two terms in the surface energy - the gradient and potential well. This also allows comparison with other postulated models as shown in Figure 19, where the surface energy at the centre of the simplex, $\phi_i = 1/3, i = 1, 2, 3$, is lower than at the binary junctions on the left but, conversely, higher for the model advocated in our paper, [28]. The other feature present

Preprints (www.preprints.org) | NOT PEER-REVIEWED | Posted: 21 December 2021 doi:10.20944/preprints202112.0346.v1

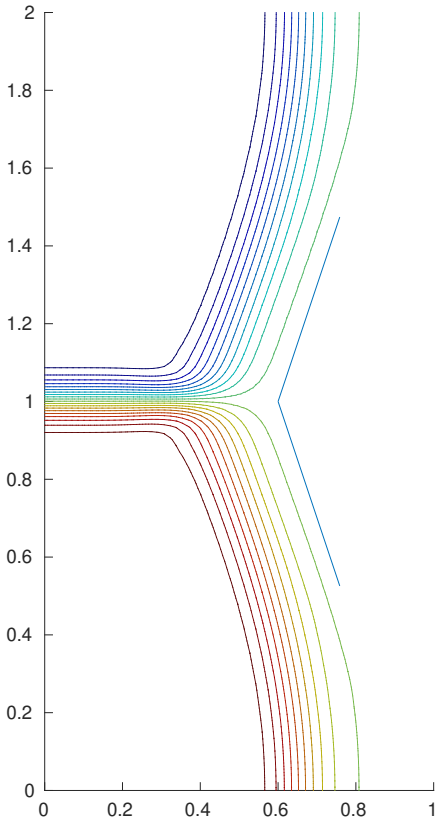

Figure 18. The contours of the phase-field align with the desired angle (here 143°).

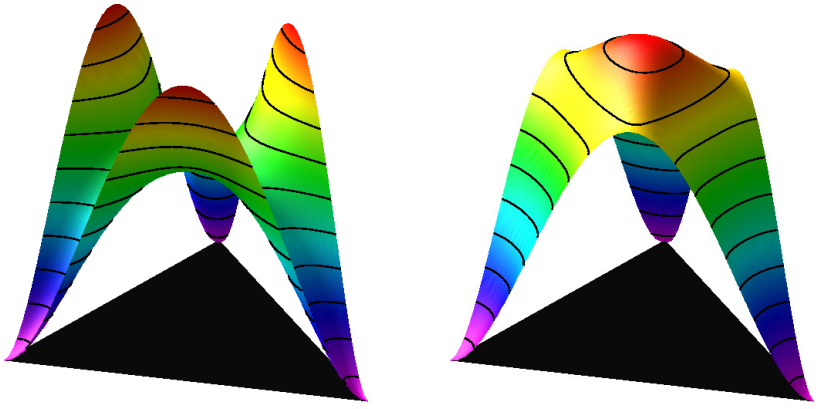

Figure 19. The two plots show the energy over a simplex as a function of three phrases, ϕ_1, ϕ_2, ϕ_3. The centre of the simplex is formally the triple junction point where, ideally, the surface energy barrier should be highest. The left plot shows the models advocated by [25] and [26] containing a hollow at the junction, whereas the model proposed by [28] (and also [23] in the special case of equal angles) has the formally correct barrier at the triple point as well as the binary junctions.

Preprints (www.preprints.org) | NOT PEER-REVIEWED | Posted: 21 December 2021 doi:10.20944/preprints202112.0346.v1

in our model (the right of Figure 19) is that the gradient of surface energy is zero at the boundary of the simplex, but this is not the case in the models advocated in [25] and [26]. A low triple junction barrier generates a spurious phase at a binary junction. The model advocated in [28] avoids both spurious phase generation and also, due to the zero gradient, does not give preference to a value outside the simplex, i.e. non-physical negative values of ϕ_i.

10. Fully coupled solute and temperature multiphase modelling

As stated in the introduction, the early days of phase-field solidification focussed on pure metal solidification and the movement towards the more interesting, from a practical engineering perspective, complex alloy solidification, came later. Because of the high conductivity of metals the temperature field can legitimately be neglected in many scenarios. That said, there are situations where the temperature field plays a crucial role in alloy solidification such as growth restriction [29], but also when the partition coefficient, $k_E \to 1$ (e.g. for almost complete solute trapping at very high growth rate), whence thermal forces exceed diffusion effects. One way of processing this is to *impose* a temperature field on the other fields, but this does not take into account the heat generation due to the volume latent heat of fusion.

In the early 2000s fully coupled single phase formulations were in existence, [3,6], but the more general fully coupled *multiphase* formulation did not. A general multiphase framework for the formulation of thermodynamically consistent phase-field models was in demand, principally to provide a temperature field equation in this more general setting. The difficulty of extending a temperature formulation from single to multiphase-field can be seen by inspecting the single phase contribution to the temperature diffusion equation,

$$C_v\dot{T} = \nabla \cdot k\nabla T + L\dot{\phi}, \tag{54}$$

where C_v is heat capacity at constant volume, k conductivity and L the latent heat. The term $L\dot{\phi}$ generates heat as the material changes phase. Now consider a plausible multiphase generalisation given by

$$C_v\dot{T} = \nabla \cdot k\nabla T + L\sum_i^n \dot{\phi}_i. \tag{55}$$

This fails because $\sum_i^n \dot{\phi}_i = 0$. A compromise might be to single out the liquid phase as *special* and write

$$C_v\dot{T} = \nabla \cdot k\nabla T + L\dot{\phi}_{\text{liquid}}, \tag{56}$$

but this undermines an implicit assumption in phase-field modelling that no phase is special - even the liquid. The other issues arising in this investigation was to question the single phase temperature equation itself. Do heat capacity and latent heat need adding to the model or do they arise naturally from the free energy? Why, in the case of binary alloys, do we not require heat generation due to solute change?

A similar set of problems arose in the modelling of complex fluids where a typical approach to model these fluids at the time was to specify the viscosity and stress tensor in terms of velocity gradients in a manner inspired by spring and dash-pot analogies, see [30]. These models and the concern that the resulting models may not be thermodynamically consistent was addressed in [5], which proposed a formalism for modelling complex fluids that closely resembled phase-field models of solidification. That is, to start the modelling by a specification of the energy and deduce the evolution equations using a modification of the Poisson bracket for continuum mechanics. We see in [31] that it turns out that one of the simplest examples of the operation of *bracket* formalism is the purely dissipative phase-field models of solidification. Particularly the isothermal single

Preprints (www.preprints.org) | NOT PEER-REVIEWED | Posted: 21 December 2021 doi:10.20944/preprints202112.0346.v1

and multiphase phase models. The formalism also shows how to recover the entropy from which it is a short step to generating a temperature equation. Then it becomes clear that the only additional parameter required to specify a temperature equation is the conductivity, k. Not only is the heat capacity and latent heat prescribed (from the free energy specification), but the addition of a term involving $\dot{c}$, similar to latent heat of fusion, also falls out of the formalism, and treatment of density change together with necessary fluid flow also is prescribed.

The n-phase formulation for the temperature field of a binary alloy, postulated in [31] is given as:

$$C_v\dot{T} = \nabla\cdot\mathbf{q} + \sum_{i=1}^{n} L_i\dot{\phi}^i + K\dot{c} \tag{57}$$

where

$$C_v \equiv -T\frac{\partial}{\partial T}\frac{\partial f}{\partial T} \tag{58}$$

$$L_i \equiv -\left(1 - T\frac{\partial}{\partial T}\right)\frac{\delta F}{\delta\phi_i} \approx -\left(1 - T\frac{\partial}{\partial T}\right)\frac{\partial f_B}{\partial\phi_i} \tag{59}$$

$$K \equiv -\left(1 - T\frac{\partial}{\partial T}\right)\frac{\partial f_B}{\partial c} \tag{60}$$

$$\mathbf{q} \equiv \kappa\nabla T + D\frac{\partial f_B}{\partial c}\nabla\frac{\partial f_B}{\partial c} \tag{61}$$

where D is the solute diffusivity. If we neglect the contributions due to solute change and gradients we have

$$C_v\dot{T} = \nabla\cdot\kappa\nabla T + \sum_{i=1}^{n} L_i\dot{\phi}^i. \tag{62}$$

This, with hindsight, seems a reasonable guess, but Eq. 59 is required to complete the definition, not only making the latent heat terms, L_i, non-constant but even differing in sign.

Finally, the general bracket formalism also poses the question as to why there is no further coupling between phase and solute concentration as would naturally occur if solute, c and the phase-fields were treated equally as part of a general vector $\boldsymbol{\phi} = [c, \phi_1, \phi_2, \phi_3]$, something that has been noted and used by other authors such as [32]. Figure 20 shows the general scheme for constructing evolution equations, that we described in [31] . The key novel part of which is that one constructs the bracket alongside the free energy. The bracket includes the diffusion parameters, which fields are conserved or not, and draws a distinction between energy conserving fields such as mass, and the dissipative dynamics as is the staple of relaxation phenomena such as solidification. Everything below the top two boxes in Figure 20 is determined by the formation of the bracket and the specification of the energy.

11. Summary

Here we summarise our main contributions to phase-field computational modelling

1. Non-linear adaptive mesh multi-grid solver for multi-scale problems [7]
2. Load balancing techniques for parallel solvers [8]
3. Control of phase-field profile to match molecular dynamic or *ab initio* calculations [10]

Preprints (www.preprints.org) | NOT PEER-REVIEWED | Posted: 21 December 2021 doi:10.20944/preprints202112.0346.v1

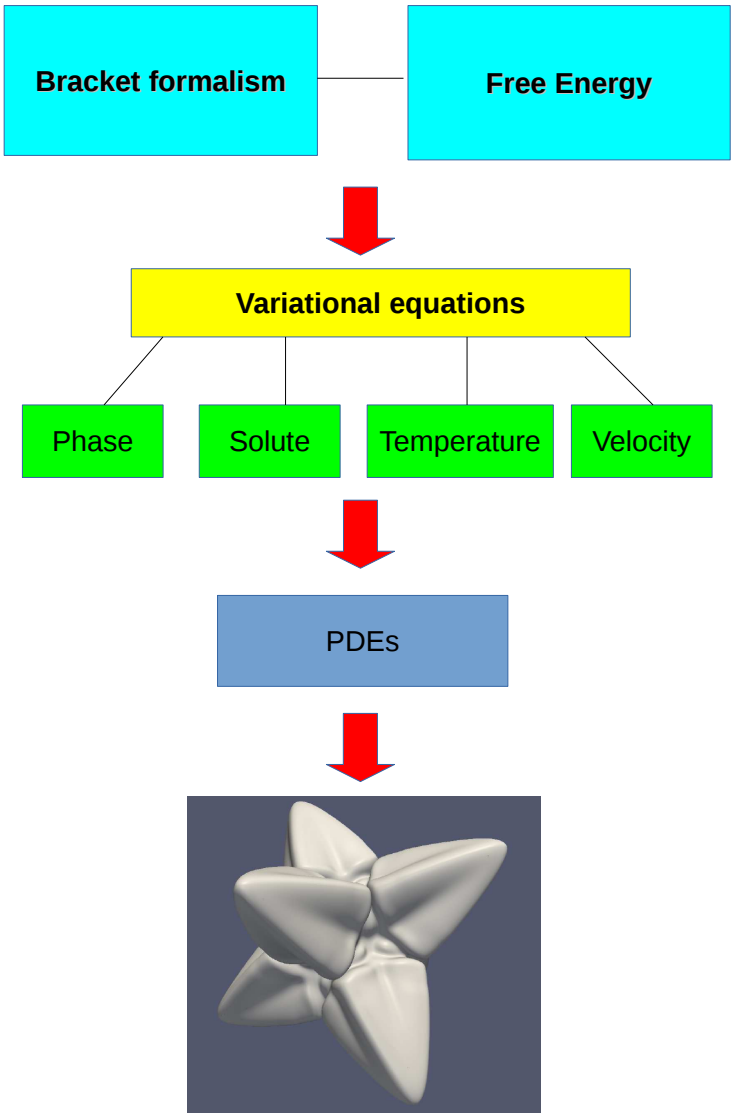

Figure 20. A diagram broadly showing the process of forming evolution equations using the bracket formalism proposed in [31] .

Preprints (www.preprints.org) | NOT PEER-REVIEWED | Posted: 21 December 2021 doi:10.20944/preprints202112.0346.v1

4. Transition from faceted (equilibrium) to dendritic morphology (non-equilibrium) [16]
5. A general approach to formulate arbitrary faceted polyhedrons and polyhedra in phase-field [12]
6. A method to give interface width independence for models using arbitrary free energy functions in single phase simulations [22]
7. Control of triple junction angle in eutectic growth [28]
8. Development of a broader formalism to give a thermodynamically consistent phase-field formulation with correct thermal field and entropy generation [31]

Appendix A Non-dimensional phase-field equations

Both the phase-field parameter, ϕ and concentration, c are dimensionless but free energy density functions provided from data bases are typically in units of Joules per mole. From Eqs. 3 and 5, a fully dimensioned form of the two-phase-field equation is of the form

$$\dot{\phi} = -M\frac{\delta F}{\delta \phi} = M\left[\nabla \cdot \frac{\partial f_S}{\partial \nabla \phi} - \frac{\partial f_B}{\partial \phi}\right] \tag{A1}$$

implying that the units of M are Moles per (Seconds$\times$ Joules), or Mol/(sJ) is S.I. units. Taking the isotropic model (see Eq. 9 for comparison) as a template for the non-dimensional procedure:

$$\begin{aligned} \dot{\phi} &= M\left[W(\delta^2\nabla^2\phi - \Omega'(\phi)) - f_B'(\phi)\right] \\ &= MW\delta^2\left[\nabla^2\phi - \frac{\Omega'(\phi)}{\delta^2} - \frac{f_B'(\phi)}{W\delta^2}\right] \end{aligned} \tag{A2}$$

where $\Omega \equiv \frac{1}{2}\phi^2(1-\phi)^2$ is a typical choice for the double well potential, and W is associated with surface energy with units adjusted to be the same as f_B. In the simplest models, the parameters, M, W and δ are all constants. Moreover, $MW\delta^2$ has the units of diffusivity and can conveniently be used as the unit of diffusivity, $MW\delta^2 \equiv D_{\text{char}}$. Writing the ratio f_B/W as $\bar{f}_B$ and using δ as the unit of length reduces the fully dimensional equation to the non-dimensional form:

$$\dot{\phi} = \nabla^2\phi - \Omega'(\phi) - \bar{f}_B'(\phi). \tag{A3}$$

This then gives the non-dimensional concentration equation as

$$\dot{c} = \nabla \cdot \bar{D}\nabla\bar{f}_B'(c) \tag{A4}$$

where

$$\bar{D} = \frac{D}{D_{\text{char}}}. \tag{A5}$$

Using these two coupled equations, we can explore a range of parameter values: M, the mobility (response of the front to the driving force); W, the coupling between surface and bulk forces; δ, the interface width, which may vary between physically based and computationally convenient. Alternatively one may fix all the constants by reference, if possible, to physically determined parameters, and then vary f_B as a function of temperature, T, to explore aspects of morphology as a function of undercooling.

Author Contributions: Conceptualization, P.C. Bollada, P.K. Jimack, A.M. Mullis; investigation, writing—original draft preparation, methodology, P.C Bollada; writing—review and editing, supervision, P.K. Jimack and A.M. Mullis; funding acquisition, project administration A.M. Mullis; All authors have read and agreed to the published version of the manuscript.

Funding: This research was funded by the EPSRC Innovative Manufacturing Research Hub in Liquid Metal Engineering (LiME), Grant No. EP/ N007638/1.

Acknowledgments: We thank the journal publishers permission to reprint the figures from our original articles in which we explicitly cite.

Conflicts of Interest: The authors declare no conflict of interest. The funders had no role in the design of the study; in the collection, analyses, or interpretation of data; in the writing of the manuscript, or in the decision to publish the results.

References

1. Karma, A.; Rappel, W. Quantitative phase-field modeling of dendritic growth in two and three dimensions. *Phys. Rev. E* **1998**, *57(4)*, 4323–4349.
2. Karma, A. Phase-Field Formulation for Quantitative Modeling of Alloy Solidification. *Phys. Rev Letters* **2001**, *87-11*, 115701.
3. Ramirez, J.C.; Beckermann, C.; Karma, A.; Diepers, H.J. Phase-field modeling of binary alloy solidification with coupled heat and solute diffusion. *Phys. Rev. E* **2004**, *69*, 051607. doi:10.1103/PhysRevE.69.051607.
4. Boettinger, W.J.; Warren, J.A.; Beckermann, C.; Karma, A. Phase-Field Simulation of Solidification. *Annual Review of Materials Research* **2002**, *32*, 163–194, [https://doi.org/10.1146/annurev.matsci.32.101901.155803]. doi:10.1146/annurev.matsci.32.101901.155803.
5. Beris, A.N.; Edwards, B.J. Thermodynamics of Flowing Systems. *Oxford University Press, New York, 1994*.
6. Rosam, J.; Jimack, P.; Mullis, A. An adaptive, fully implicit multigrid phase-field model for the quantitative simulation of non-isothermal binary alloy solidification. *Acta Materialia* **2008**, *56*, 4559–4569. doi:https://doi.org/10.1016/j.actamat.2008.05.029.
7. Bollada, P.C.; Goodyer, C.E.; Jimack, P.K.; Mullis, A.M.; Yang, F.W. Three Dimensional Thermal-Solute Phase Field Simulation of Binary Alloy Solidification. *J. Comp. Phys.* **2015**, *287*, 130–150.
8. Chen, M.H.; Bollada, P.; Jimack, P. Dynamic Load Balancing for the Parallel, Adaptive, Multigrid Solution of Implicit Phase-Field Simulations. *International Journal of Numerical Analysis and Modeling* **2019**, *16*, 297–318.
9. Yang, F.W.; Goodyer, C.E.; Hubbard, M.E.; Jimack, P.K. An optimally efficient technique for the solution of systems of nonlinear parabolic partial differential equations. *Advances in Engineering Software* **2017**, *103*, 65–84.
10. Bollada, P.; Men, H.; Fang, C.; Jimack, P.; Fan, Z.; Mullis, A. A novel route to the coupling of molecular dynamics and phase-field simulations of crystal growth. *IOP Conference Series: Materials Science and Engineering* **2019**, *529*, 012032. doi:10.1088/1757-899X/529/1/012032.
11. Takaki, T.; Sakane, S.; Ohno, M.; Shibuta, Y.; Shimokawabe, T.; Aoki, T. Primary arm array during directional solidification of a single-crystal binary alloy: Large-scale phase-field study. *Acta Materialia* **2016**, *118*, 230 – 243. doi:https://doi.org/10.1016/j.actamat.2016.07.
12. Bollada, P.C.; Jimack, P.K.; Mullis, A.M. A vertex based approach to crystal facet modelling in phase field. *Computational Materials Science* **2021**, *192*, 110331.
13. Salvalaglio, M.; Backofen, R.; Bergamaschini, R.; Montalenti, F.; Voigt, A. Faceting of Equilibrium and Metastable Nanostructures: A Phase-Field Model of Surface Diffusion Tackling Realistic Shapes. *Crystal Growth & Design* **2015**, *15*, 2787–2794, [https://doi.org/10.1021/acs.cgd.5b00165]. doi:10.1021/acs.cgd.5b00165.
14. Eggleston, J.; McFadden, G.; Voorhees, P. A phase-field model for highly anisotropic interfacial energy. *Physica D: Nonlinear Phenomena* **2001**, *150*, 91 – 103. doi:https://doi.org/10.1016/S0167-2789(00)00222-0.
15. Yuan, X.f.; Liu, B.y.; Li, C.; Zhou, C.s.; Ding, Y.t. Simulation of facet dendrite growth with strong interfacial energy anisotropy by phase field method. *Journal of Central South University* **2015**, *22*, 855–861. doi:10.1007/s11771-015-2593-8.
16. Bollada, P.; Jimack, P.; Mullis, A. Faceted and dendritic morphology change in alloy solidification. *Computational Materials Science* **2018**, *144*, 76 – 84. doi:https://doi.org/10.1016/j.commatsci.2017.12.007.
17. Wheeler, A.; Boettinger, W.; McFadden, G. Phase-field model for isothermal phase transitions in binary alloys. *Physical Review A* **1992**, *45(10)*, 7424–7440.
18. Kim, S.G.; Kim, W.T.; Suzuki, T. Phase-field model for binary alloys. *Phys. Rev E* **1999**, *60(6)*, 7186–7197.
19. Bollada, P.C.; Jimack, P.K.; Mullis, A.M. Free energy vs. Grand Potential Energy formulations in phase field modelling of alloy solidification. *Proceedings of the 7th International Conference on Solidification & Gravity* **2018**, pp. 47–51.
20. Plapp, M. Unified derivation of phase-field models for alloy solidification from a grand-potential functional. *Phys. Rev. E* **2011**, *84*, 31601.
21. et al, S.G.K. *J. Crystal Growth* **2004**, *261*, 135–158.
22. Bollada, P.; Jimack, P.K.; Mullis, A.M. A numerical approach to compensate for phase field interface effects in alloy solidification. *Computational Materials Science* **2018**, *151*, 338–350.
23. Folch, R.; Plapp, M. Towards a quantitative phase-field model of two-phase solidification. *Phys. Rev. E* **2003**, *68*, 010602.
24. Bollada, P.C.; Jimack, P.K.; Mullis, A.M. A new approach to multi-phase formulation for the solidification of alloys. *Physica D* **2012**, *241*, 816–829.
25. Tiaden, J.; Nestler, B.; Diepers, H.J.; Steinbach, I. The muiltiphase-field model with an integrated concept for modelling diffusion. *Physica D* **1998**, *115*, 73–86.
26. Nestler, B.; Wheeler, A.A. A multi-phase-field model of eutectic and peritectic alloys: numerical simulation of growth structures. *Physica D* **2000**, *138*, 114–133.

27. Toth, G.I.; Pusztai, T.; Granasy, L. Consistent multiphase-field theory for interface driven multidomain dynamics. *Phys. Rev. B* **2015**, *92*, 184105.
28. Bollada, P.; Jimack, P.; Mullis, A. Multiphase field modelling of alloy solidification. *Computational Materials Science* **2020**, *171*, 109085. doi:https://doi.org/10.1016/j.commatsci.2019.109085.
29. Greer, A. *Phil. Trans. R. Soc. A* **2003**, *361*, 475–495.
30. Owens, R.G.; Phillips, T.N. Computational Rheology. *Imperial College Press* **2002**.
31. Bollada, P.C.; Jimack, P.K.; Mullis, A.M. Bracket formalism applied to phase field models of alloy solidification. *Comp. Mat. Sci* **2017**, *126*, 426–437.
32. Brener, E.A.; Boussinot, G. Kinetic cross coupling between nonconserved and conserved fields in phase field models. *Phys Rev E* **2012**, *86*, 060601.